

1 **Air pollution reductions caused by the COVID-19 lockdown open up a way to preserve**
2 **the Himalayan Glaciers**

3 Suvarna Fadnavis^{1*}, Bernd Heinold², T. P Sabin¹, Anne Kubin², Katty Huang³, Alexandru
4 Rap⁴, and Rolf Müller⁵

5 ¹Indian Institute of Tropical Meteorology, Centre for climate change research, Ministry of
6 Earth Sciences, India

7 ²Leibniz-Institut für Troposphärenforschung, Leipzig, Germany,

8 ³Urban Climate, Risk & Health, UCL, London, United Kingdom

9 ⁴School of Earth and Environment, University of Leeds, Leeds, UK,

10 ⁵Forschungszentrum Jülich GmbH, IEK-7, Jülich, Germany,

11 Corresponding author email: suvarna@tropmet.res.in

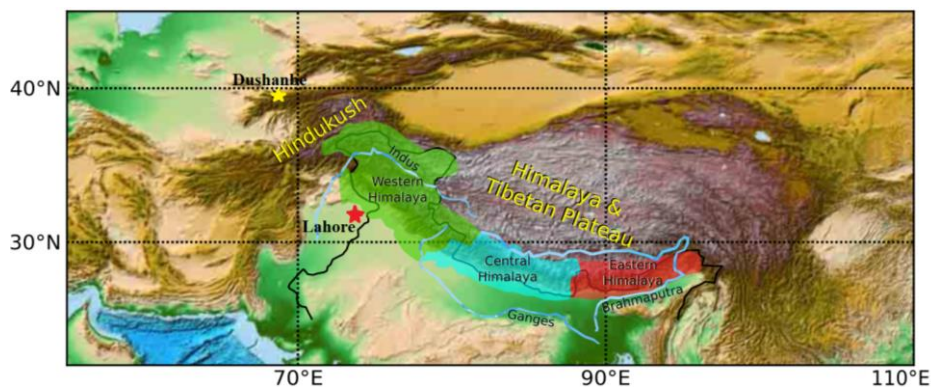
12 Abstract

13 The rapid melting of glaciers in the Hindu Kush Himalayas (HKH) during recent decades
14 poses an alarming threat to water security for larger parts of Asia. If this melting persists, the
15 entire Himalayan glaciers are estimated to disappear by end of the 21st century. Here, we
16 assess the influence of the spring 2020 COVID-19 lockdown on the HKH, demonstrating the
17 potential benefits of a strict emission reduction roadmap. Chemistry-climate model
18 simulations, supported by satellite and ground measurements, show that lower levels of gas
19 and aerosol pollution during lockdown led to changes in meteorology, and to a reduction in
20 black carbon in snow (2-14%) and thus in snow melting (10-40%). This caused increases in
21 snow cover (6-12%) and mass (2-20%) and a decrease in runoff (5-55%) over the HKH and
22 Tibetan Plateau, ultimately leading to an enhanced snow-equivalent-water (2–55%). We
23 emphasize the necessity for immediate anthropogenic pollution reductions to address the
24 hydro-climatic threat to billions of people in South Asia.

25

26 **1. Introduction**

27 The Hindu Kush Himalayan (HKH) mountains and Tibetan plateau is the largest snow-cladded
28 region outside the Poles (Fig. 1). This region is also referred to as High Mountain Asia,
29 although that includes the Tien Shan and some other northern ranges. The HKH meltwater
30 feeds rivers in India and China that drive the agriculture, hydropower generation, and economy
31 of these countries (Hussain et al., 2019; Sabin et al., 2020; Lee et al. 2021a). The Himalayan
32 snowmelt in spring provides ~50% of the annual freshwater to ~4 billion people of South Asia
33 and East Asia (Sarangi et al 2019, Sabin et al., 2020). Rapid Himalayan snowmelt caused a
34 loss of ~40 % of the Himalayan glacier area compared to the Little Ice Age, 400 to 700 years
35 ago, i.e. ~0.92 to 1.38 mm sea-level equivalent (Lee et al., 2021b). The snow mass over the
36 Himalayas has generally decreased during the last 30 years (except for a few Karakoram
37 glaciers that show an increasing trend in snow mass) (Hussain et al., 2019. The alarming rate
38 of snow melting of 0.02 to 0.6 cm °C⁻¹ day⁻¹ raised concerns about the sustainability of water
39 supply (Tiwari et al., 2015) and loss of glaciers in the region (Hussain et al., 2019, Lee et al.,
40 2021b). Model simulations for extreme scenarios show that Himalaya snow melting could
41 cause the glaciers to disappear by the end of the 21st century (Cruz et al. 2007, Hock et al.,
42 2019).



47 **Figure 1:** Map of the Hindu Kush Himalayas region with the Western (70 - 80° E, 30° - 35° N),
48 Central (80° - 87° E, 28° - 30° N), and Eastern Himalayas (88° - 95° E, 26° - 30° N). A yellow
49 and red star indicates the location of the AERONET sun photometer stations Dushanbe
50 (68.858° E, 38.553° N) and Lahore (74.264° E, 31.480° N), respectively.

51 The accelerated thinning of Himalayan glaciers is attributed to climate change causing
52 shifts in air temperature and precipitation, as well as the atmospheric distribution and
53 deposition of light-absorbing particles i.e., dust and black carbon (BC) (IPCC Climate Change
54 2013, Krishnan et al., 2019). Among the aforementioned factors, snow darkening due to the
55 deposition of absorbing aerosols is an integral component of Himalayan snowmelt and runoff
56 (Lau et al., 2010). The snow-melting efficacy of BC is higher than that of greenhouse gases
57 (Qian et al., 2011; Nair et al. 2013; Ma et al., 2019; Sarangi et al., 2019). The increasing energy
58 demand of the densely populated South Asian region has increased the emission of greenhouse
59 gases and BC aerosol in the last few decades (Fadnavis et al., 2017, Krishnan et al., 2020),
60 leading to enhanced darkening and snow melting (Usha et al., 2021).

61

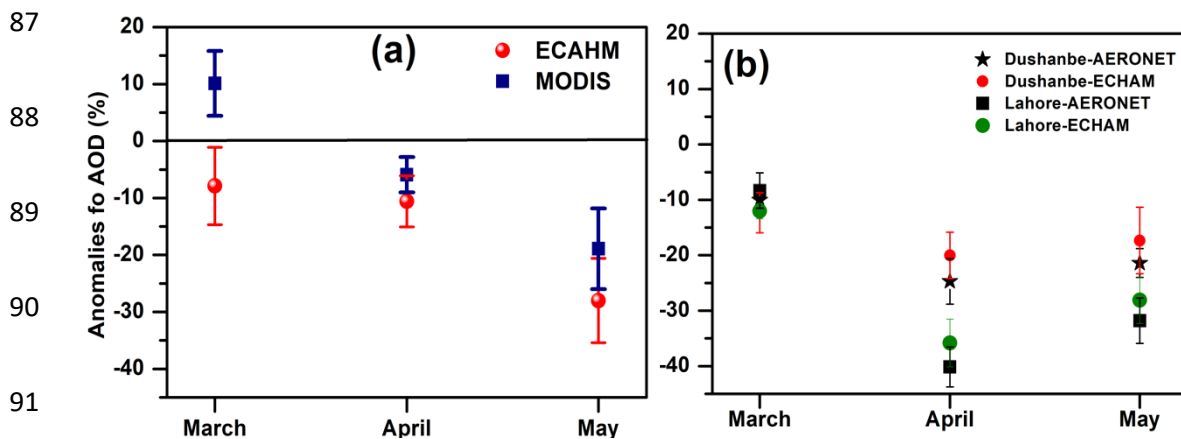
62 The economic slowdown caused by the COVID-19 pandemic measures led to a drastic
63 reduction in public and freight transportation, industrial emissions, and energy use (Fadnavis
64 et al., 2021a). This resulted in a substantial decline in emissions of several atmospheric
65 pollutants including greenhouse gases and black carbon aerosol (Forster et al. 2020; Kanniah
66 et al., 2020; Le Quéré et al 2020), and potentially reduced deposition of dark aerosols on snow
67 and ice (Bair et al., 2021). Remote sensing approaches show cleaner snow with ~30% less
68 light-absorbing impurities in snow during the lockdown period over Asia between March and
69 May 2020 (Bair et al 2021). This led to decreased snowmelt by 25 – 70 mm in 2020 compared
70 to the last 20-year mean for March-May over Western Himalayas due to decreased radiative
71 forcing induced by BC and dust deposition on snow/ice surfaces and related changes in snow
72 absorption and surface albedo (Bair et al., 2021). Bair et al. (2021) also found that 6.6 km⁻³ of
73 melt water stayed in the Indus Basin. Gauge and reservoir data for this part of the world,
74 however, are not freely available. Impacts of reduced levels of air pollution on changes in the
75 snow mass, surface water runoff, and water reservoir over the HKH are not reported hitherto.

76 Here, we provide a detailed analysis of the impact of reduced pollution over HKH and Tibetan
 77 plateau region during the COVID-19 lockdown period between March and May 2020. We used
 78 global simulations with the chemistry-climate model ECHAM6-HAMMOZ (Schultz et al.,
 79 2018, Tegen et al., 2019), updated with an improved BC-in-snow parameterization (Huang
 80 2018), in order to contrast the 2020 COVID-19 (COVID) with the typical, unchanged (control,
 81 CTL) air pollution conditions. The COVID simulations are performed using a COVID-19
 82 emission inventory where emissions are reduced based on Google and Apple mobility data
 83 (Forster et al., 2020; details in section S1).

84

85 2 Results

86 2.1 Reduction of airborne aerosols and in-snow BC concentration over the Himalayas



92 **Figure 2:** (a) Changes in monthly mean AOD (%) during March - May 2020 from MODIS in
 93 comparison to mean of 2001-2019 and ECHAM-HAMMOZ (COVID minus CTL) averaged
 94 over the Hindu Kush Himalayas (HKH) and Tibetan Plateau region (75° - 95° E, 30° - 35° N),
 95 (b) same as (a) but for AOD from AERONET observations and ECHAM-HAMMOZ model
 96 results at Dushanbe (68.858° E, 38.553° N, climatology 2010-2019) and Lahore (74.264° E,
 97 31.480° N, climatology 2006-2019). Vertical bars in Fig (a)-(b) indicate the standard deviation
 98 within ten members of model simulations, and within monthly mean anomalies from MODIS
 99 for years 2001-2019.

100

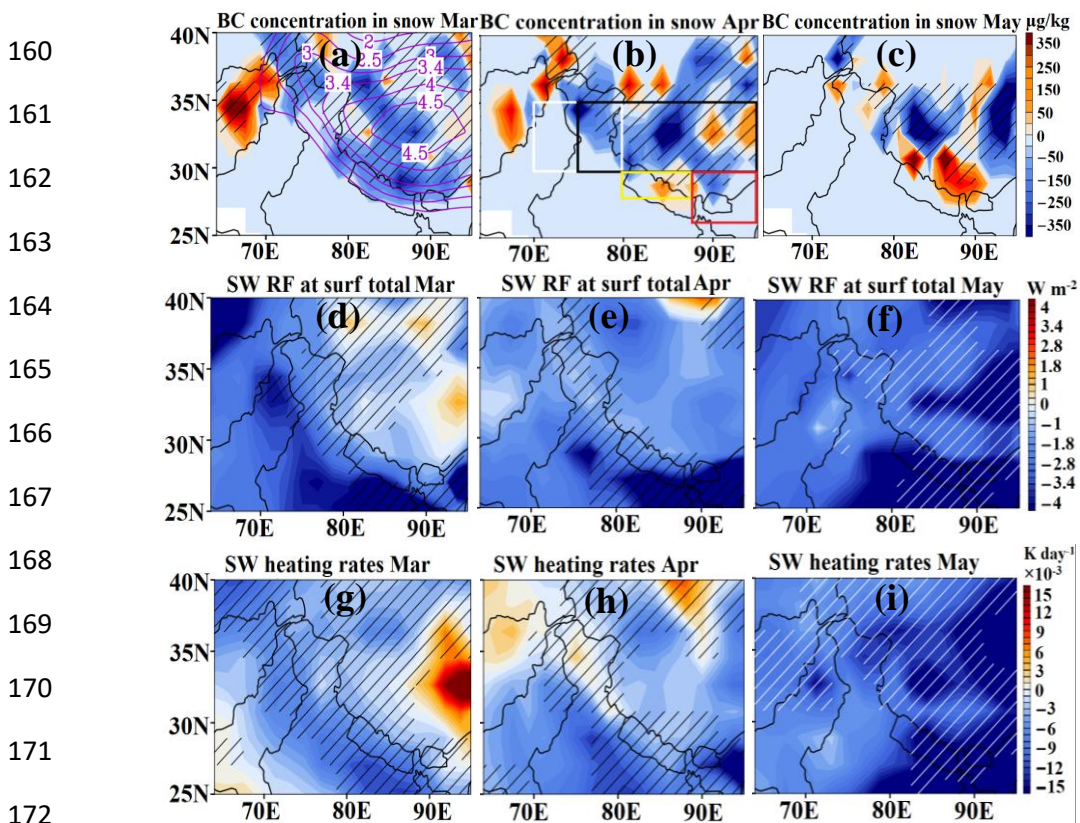
101 The COVID-19 lockdown restrictions in spring 2020 decreased the anthropogenic
102 aerosol amounts over the HKH ranges (Western, Central, and Eastern Himalayas), and the
103 Tibetan Plateau region. The ECHAM6-HAMMOZ model simulations show that COVID
104 lockdown resulted in a cleaner atmosphere during March - May 2020 over the HKH ranges and
105 Tibetan Plateau region. There is a reduced level of Aerosol Optical Depth (AOD) over the
106 region throughout spring 2020 by $-8.1\pm 6.2\%$ in March, $-10.2\pm 4.7\%$ in April, $-27\pm 6.9\%$ in
107 May compared to the CTL (non COVID) simulation (Fig. 2a). This is supported by NASA's
108 Moderate Resolution Imaging Spectroradiometer (MODIS) measurements also showing a
109 reduction in AOD in April ($-5.6\pm 3.3\%$) and May ($-18.8\pm 7.2\%$) 2020 compared to the mean
110 over the last 20 years (Fig. 2a). Thus, both model simulations and MODIS AOD show a
111 reduction in aerosol pollution in April - May 2020. For March 2020, MODIS measurements
112 show AOD enhancement by $10.2 \pm 4.8\%$, which is due to increased dustiness over the HKH
113 region (see section S2 for a detailed discussion). AOD measurements at two Aerosol Robotic
114 Network (AERONET) sun photometer stations in Dushanbe (68.858° E, 38.553° N)
115 and Lahore (74.264° E, 31.480° N) show an AOD reduction in agreement with our model
116 simulations (Fig. 2b). There are differences among MODIS, AERONET and the model. The
117 changes in AOD during COVID compared to no-COVID period is less in the model than the
118 MODIS observations by 4.2 - 9.8 % and higher than the AERONET observations by 1.8 - 4.2
119 %. These differences are due to the fact that the simulated AOD change is in response to the
120 reduction of anthropogenic aerosols and associated circulation responses, while MODIS and
121 AERONET measurements show the effect of all atmospheric processes. Also, note that the
122 MODIS AOD values are spatial averages representative for a relatively large area while the
123 AERONET values are point measurements. Importantly, changes in simulated AOD in 2020
124 fall within the standard deviation of satellite and ground-based measurements indicating
125 reliability of our simulations (except for March 2020 with respect to MODIS). Our model

126 simulations also show a reduction in BC burden by 15 - 55% (Fig. S1a), and sulfate burden by
127 22 - 24 % over the HKH and Tibetan Plateau regions in spring 2020 (Fig. S1b). Interestingly,
128 dust burden also shows a reduction over these regions (Fig. S1c, Fig. S2a-c), except over central
129 Himalaya in March and April 2020. The lower dust load is related to the interactive change in
130 atmospheric dynamics in the model, which also leads to changes in the wet and dry deposition
131 rates of dust (Fig. S2d-i) (details in section S2). A drop in BC is also observed in Aerosol
132 Radiative Forcing Over India Network (ARFINET) ground-based measurements over the Indo-
133 Gangetic Plain (> 50 %), north-eastern India (>30%), Himalaya regions (16 - 60%), and Tibet
134 (70%) during spring 2020 (Gogoi et al., 2021; Liu et al., 2021). A similar impact of the
135 reduction of energy consumptions on decrease in AOD during the COVID-19 lockdown period,
136 i.e., in spring 2020 compared to the 2010-2019 climatology is also seen over South and East
137 Asia (40 %) and the Indo-Gangetic Plain (IGP) by 30 – 40 % in satellite measurements
138 (Fadnavis et al., 2021a; Srivastava et al., 2021; Pandey et al., 2021; Shafeeque et al., 2021).

139

140 The reduction in anthropogenic air pollution leads widely to a reduction in BC
141 concentration in the snow of approximately 25 - 350 $\mu\text{g kg}^{-1}$ (by 12 – 35 %) during spring 2020
142 (Fig. 3a-c) that reduce the snow darkening effect by embedded aerosol impurities. At the most
143 this amounts to about a 1.6% increase in visible snow albedo. Sporadically, however, the BC-
144 in snow concentrations have also increased in some areas of the Hindukush, Eastern Himalayas
145 and Kunlun Mountains. There are many factors at play that may lead to an increase in BC
146 concentration in snow in some locations. For instance, this includes increases in deposition of
147 BC following shifts in the atmospheric circulation (Fig.S3), accumulation of BC on surface
148 snow following partial snowmelt and minimal fresh snowfall, and less frequent occurrences of
149 complete snowmelt which would otherwise remove all accumulated BC in snow. Our
150 simulations reveal that the decrease in BC-in snow concentration and the overall reduction in

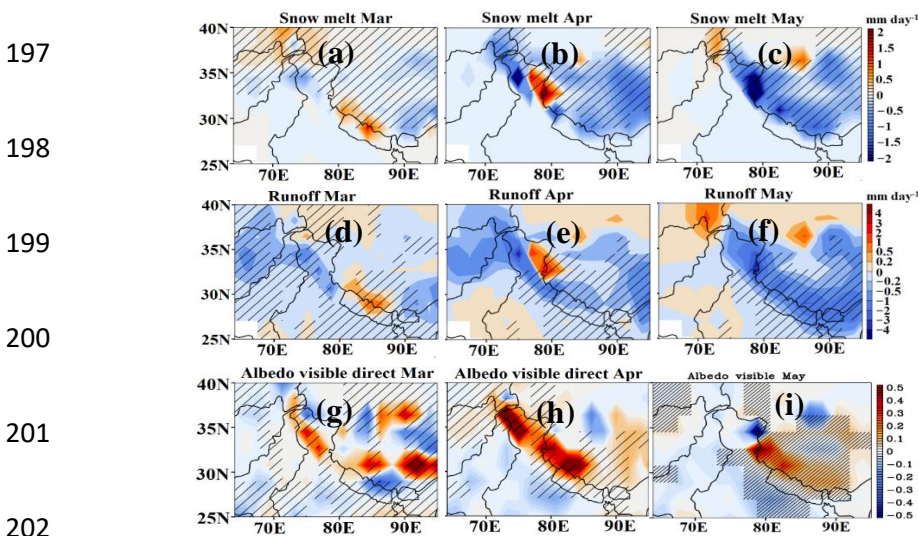
151 atmospheric pollution, as well as associated radiative effects have decreased the shortwave
 152 radiative forcing at the surface by $0.2 - 2 \text{ W m}^{-2}$ in March – May 2020 (Fig. 3 d-f), leading to
 153 a decrease in tropospheric heating by solar radiation of 0.001 to 0.015 K day^{-1} (Fig. 3 g-i). The
 154 reduced anthropogenic BC over the HKH and Tibetan Plateau region resulted in less absorption
 155 and re-emission of longwave radiation and, as a consequence, there is a reduction in longwave
 156 radiative forcing in the atmosphere leading to a lower atmospheric heating (Fig. S4). Therefore,
 157 the reduction of anthropogenic sulfate, and BC burden, combined with lower atmospheric
 158 loadings of PM_{2.5} and PM₁₀, as well as BC in snow resulted in decreased heating of the
 159 snowpack and tropospheric column.



173 **Figure 3:** Spatial distribution of anomalies (COVID minus CTL) of BC concentration in snow
 174 ($\mu\text{g kg}^{-1}$) for (a) March, (b) April, and (c) May 2020; (d-f) shortwave radiative forcing (W m^{-2})
 175 at the surface and (e-g) tropospheric heating rates (K day^{-1}) due to changes in BC
 176 concentration in snow (COVID minus CTL). Hatched areas indicate the 95%-significance
 177 level. Contours in panel (a) indicate topography in km. Boxes in panel (b) indicate boundaries
 178 of Western Himalayas (WH, white), Central Himalayas (CH, yellow), Eastern Himalayas (EH,
 179 red) and Tibetan Plateau (black).

180 2.2 Impacts on snow melting, surface water runoff, and snow cover

181 Further we show that the decrease in aerosol pollution reduced the snow melting in
182 spring 2020 by 0.2 to 2.5 mm day⁻¹ corresponding to 10 – 50 % (Fig. 4 a-c). The amount of
183 reduction of snow melting is pronounced over the western Himalayas in May. As a result of a
184 reduction in snowmelt, surface water runoff has been drastically reduced by 2-4 mm –ay⁻¹ (5 -
185 55 %) (Fig. 4 d-f). The reduction in the runoff is most pronounced in May over the entire
186 Himalayas and central Tibetan Plateau region. Estimates from remote sensing measurements
187 also show the reduction of runoff by 6.5 km³ of melted water in the Indus River Basin (Bair et
188 al. 2020). In the past, studies have shown that elevated levels of light-absorbing aerosols
189 (elemental carbon: 13 to 75 ng g⁻¹ and dust: 32 to 217 μg g⁻¹) can contribute to about 3 to
190 10 mm day⁻¹ of snowmelt over western Himalayas (Thind et al. 2019). A sensitivity analysis
191 using a glacier mass balance model shows that a BC-induced snow albedo reduction (Fig. 4 g-
192 i) resulted in an increase in runoff by 4 – 18% annually (Santra et al., 2019). In contrast to
193 impacts of rising anthropogenic emissions during the past decades, emission reductions during
194 the 2020 COVID-19 lockdown period caused a brighter snow albedo and therefore an enhanced
195 surface reflection with albedo increases of 0.2 - 0.5 (see Fig. 4g-i), leading to less atmospheric
196 heating as well as associated reduced snowmelt and surface water runoff in spring 2020.



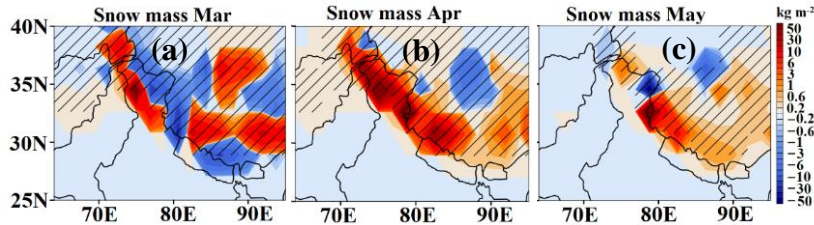
203 **Figure 4:** Spatial distribution of anomalies of (a-c) snow melt (mm day^{-1}), (d-f) surface water
 204 runoff (mm day^{-1}) for March to May 2020 (COVID minus CTL) and (g-i) surface albedo mean
 205 in the visible. Hatched areas indicate the 95%-significance level.

206

207

208

209

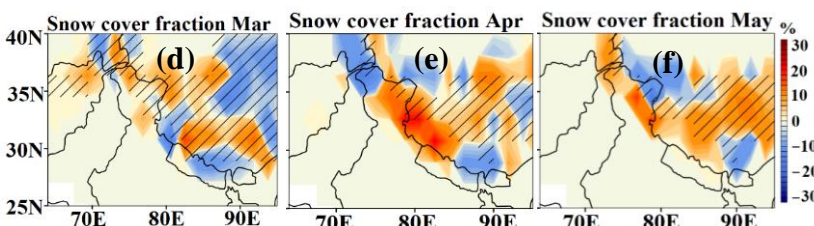


ECHAM snow cover

210

211

212

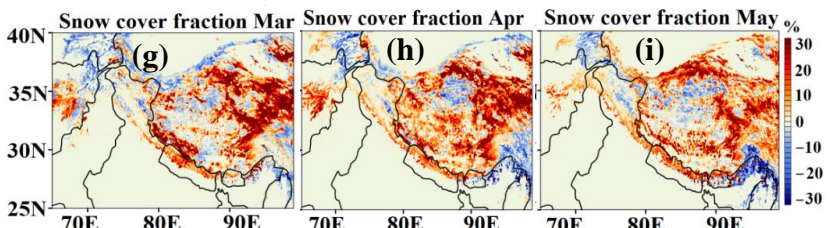


MODIS snow cover

213

214

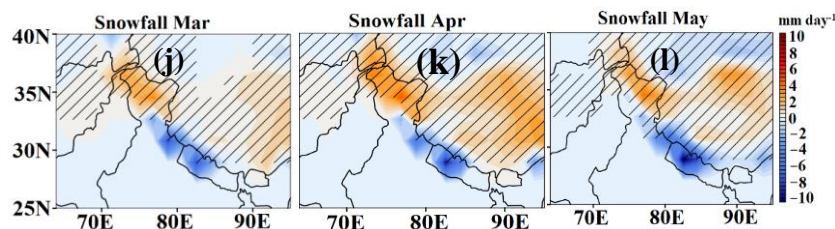
215



216

217

218



219 **Figure 5:** Monthly mean anomalies (COVID minus CTL) for March to May 2020 of (a-c) the
 220 snow mass (kg m^{-2}), (d-f) snow cover fraction (%) as modelled by ECHAM6-HAMMOZ as
 221 well as (g-i) snow cover fraction from MODIS satellite measurements (%) with respect to the
 222 climatological average 2000-2019, and, (j-l) snowfall as modelled by ECHAM6-HAMMOZ.
 223 Hatched areas indicate the 95%-significance level.

224

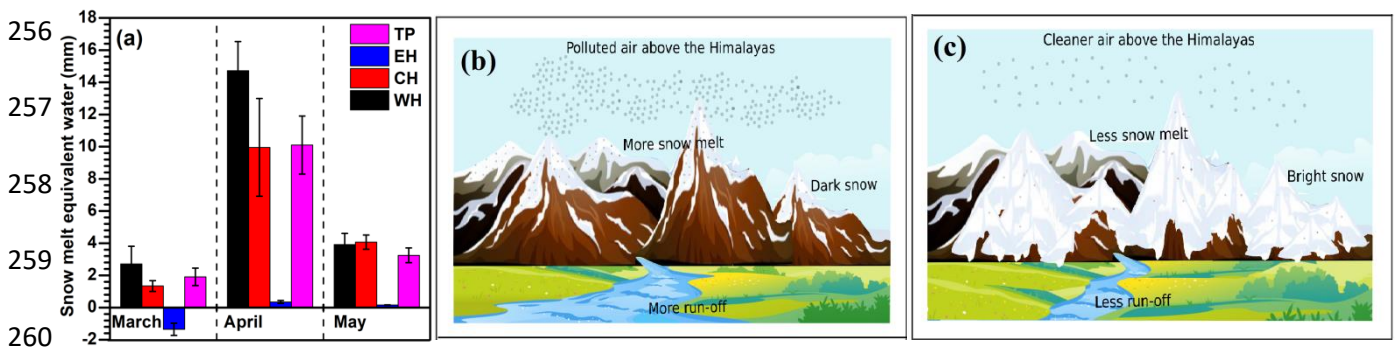
225 Our simulations also indicate that these changes lead to an increase in snow mass of
 226 $0.2\text{-}50 \text{ kg m}^{-2}$, i.e. 10-40% (Fig. 5a-c) and snow cover fraction of 2-30% during spring 2020
 227 (Fig. 5d-f). MODIS measurements also show a remarkable agreement with the model
 228 simulations (especially during April - May 2020), with increased snow cover of about 15-30%

229 over the parts of Western Himalayas and Central Himalayas and the Tibetan Plateau region
230 and decreased by 5-12 % over parts of North-East Himalayas especially in April and May 2020
231 (Fig. 5 g-i). However, there are also some differences in terms of exact regions of snow cover
232 enhancement or reduction respectively, since the MODIS observations include the influence of
233 real-time meteorology, while meteorology in the model ensemble include internal variability
234 and do not replicate the exact conditions observed by MODIS. Our model simulations show
235 that air pollution reductions in the COVID-19 lockdown period and associated changes in
236 radiative forcing caused changes in the tropospheric circulation and thermodynamics (see
237 Fadnavis et al., 2020 for a detailed analysis). These changes in meteorology have increased
238 snowfall by 2-5 mm day⁻¹ (3-20 %) over the Western Himalayas and Tibetan Plateau region
239 (Fig. 5 j-l). The increase in snowfall over these regions will contribute to enhancement in snow
240 mass and snow cover (Fig. 5 a-f) and albedo (Fig. 4 g-i). In a few areas, however, this also
241 contributes to a more efficient BC deposition on snow, as described above (Fig. 3), but this
242 does not affect the overall conclusion as to the albedo effect.

243

244 Himalaya snow is the largest source of freshwater for South Asia (Bolch et al., 2012).
245 The impact of reduced pollution on the surface water content in the Himalayas from our model
246 simulations is illustrated in Fig. 6a. The snow mass enhancement led to increase the snow
247 equivalent water by 2 to 14.7 mm (2.5 to 55 %). The western Himalayas show the highest
248 increase in snow equivalent water by 14.7 mm (55 %) followed by the Tibetan Plateau by 12
249 mm (by 22 %) and central Himalayas by 10 mm (by 18%) in April while the Eastern Himalayas
250 show a decrease in March (-1.3 mm; 10 %) and small enhancement in April by 1.1mm (2.3 %)
251 and May 2020 by 1.3 mm (2.7%) due to pollution reduction. Thus, human induced pollution
252 reduction during the COVID-19 lockdown benefitted the HKH in many ways. A schematic
253 shows the COVID-19 lockdown-induced effects in Figs. 6b-c: increased snow surface

254 reflectivity, reduced snowmelt and surface water runoff, as well as enhanced water content in
 255 the reservoir and snow.



261 **Figure 6:** (a) Change in water content (mm) of the Himalayan surface reservoirs (COVID
 262 minus CTL) from March to May 2020 over the Western Himalayas (WH), Central Himalayas
 263 (CH), Eastern Himalayas (EH) and Tibetan Plateau (TP). Vertical bars indicate the standard
 264 deviation within ten members of model simulations. Schematic illustrating the impacts of (b)
 265 air pollution on snow darkening in the Himalayas and surface water runoff for the usual
 266 polluted case and (c) the impacts of reduced pollution on snow brightening in the Himalayas
 267 and reduced surface water runoff, as observed during the 2020 COVID-19 lockdown period.

268

269 **3. Summary and conclusions:** A rising trend in Asian air pollution and associated

270 climate change over the last few decades has had a detrimental impact on snow melting over
 271 the Hindu Kush Himalayas (HKH) and Tibetan Plateau region (Wester et al., 2019). Black
 272 carbon from increasing emissions of biomass burning, industrial and domestic combustion and
 273 transport is deposited on snow, reducing its albedo (i.e. darkening) (Bolch et al., 2019). A snow
 274 darkening effect, compounded with other climate change effects, accelerates the melting of
 275 snow and the disappearance of ice cover over the HKH and Tibetan Plateau region at an
 276 extraordinary rate (Usha et al., 2021). The drop in anthropogenic air pollution emissions, e.g.
 277 from energy production, during the COVID-19 lockdown period in spring 2020 reduced air
 278 pollutant levels worldwide (Forster et al., 2020). Our model simulations indicate that the
 279 associated reduction in anthropogenic aerosols and greenhouse gases in spring 2020 has
 280 benefited the HKH snow reservoirs. It caused an enhancement in the snow cover fraction by 6

281 - 12 % and snow mass by 2 - 20 %, corresponding to a decrease in snow melting by 10 - 40%
282 and surface water runoff by 0.2 - 3 mm day⁻¹. As a consequence, the water content of the
283 reservoir increased considerably by 4 to 59 %.

284 Our findings highlight that out of the two processes causing a retreat of Himalayan glaciers:
285 (1) a slow response to global climate change and (2) a fast response to local air pollution
286 (especially black carbon), a policy action on the latter is more likely to be within reach of
287 possible policy action on a shorter-term time scale and a more regional spatial scale. Even if
288 we stopped CO₂ emissions immediately, temperatures would not start decreasing. Our findings
289 confirm the importance of reducing short-lived climate forcers (black carbon) and their
290 complementary role to CO₂ mitigation (Rogelj et al., 2014). Reduction of air pollution to levels
291 similar with those recorded during the 2020 COVID-19 lockdown period, could safeguard
292 HKH glaciers, which are otherwise under the threat to disappear by the end of the 21st century.
293 Since 2000 Himalayan glaciers have been losing nearly half a meter of ice per year (Wester et
294 al., 2019). Our estimates indicate that air pollution reduction during COVID 19 lockdown in
295 spring 2020 caused a reduction in snow melt by 0.5 to 1.5 mm day⁻¹, indicating large benefits
296 to HKH glaciers. Even if global warming is kept below 1.5°C, one third of the glaciers in the
297 HKH region and more than half of those in the Eastern Himalaya will likely be lost by the end
298 of this century (Bolch et al., 2019). The speedily retreating glaciers and the snowpack loss are
299 already posing a threat to domestic sustainable water resources for billions of people in Asia
300 (Wood et al., 2021). However, if new economically and technically feasible policies would
301 reduce emissions of air pollutants (in particular black carbon) to at least lockdown period
302 levels, snowmelt could be reduced by 10 – 50%. Such policies will therefore bring substantial
303 benefits for sustained water supply, agriculture, and ecosystems in large parts of Asia.

304

305 **Section S1: Methods:**

306 S1.1 Observational data

307 We used monthly snow cover fraction from NASA's Moderate Resolution Imaging
308 Spectroradiometer (MODIS) satellite product on a $0.5 \times 0.5^\circ$ resolution (version 6, level 3; Hall
309 et al., 2006) for the years 2000 – 2020 (<https://nsidc.org/data/MOD10CM/versions/6>). For
310 aerosol information we used monthly mean satellite AOD at $1 \times 1^\circ$ resolution from the MODIS
311 Terra level-3 dark target and deep blue retrievals at 550 nm wavelength for 2001-2020
312 (<https://giovanni.gsfc.nasa.gov>). Uncertainty in MODIS AOD data over snow are documented
313 by Huang et al (2020). We also used ground-based sun photometer observations of AOD from
314 the Aerosol Robotic Network (AERONET) (Martonchik et al., 2004) at the stations Dushanbe
315 (68.858° E, 38.553° N) for the period 2010-2020 and Lahore (74.264° E, 31.480° N) for the
316 period 2006 – 2020, situated in HKH region (<https://aeronet.gsfc.nasa.gov>).

317

318 **S1.2 The ECHAM6-HAMMOZ model description and Experimental set-up**

319 We performed 10-member ensemble experiments using the state-of-the-art aerosol-
320 chemistry-climate model ECHAM6-HAMMOZ (version echam6.3-ham2.3-moz1.0; Schultz et
321 al., 2018, Tegen et al., 2019). The model comprises the atmospheric general circulation model
322 ECHAM6 (Stevens et al., 2013), the atmospheric chemistry module MOZ (Schultz et al, 2018),
323 and the Hamburg Aerosol Model (HAM; Stier et al., 2005; Zhang et al., 2012). The HAM
324 component predicts the nucleation, growth, evolution, and sinks of sulphate (SO_4^{2-}), black
325 carbon (BC), particulate organic matter (POM), sea salt (SS), and mineral dust (DU) aerosols.
326 Seven log-normal modes describe the size distribution of the aerosol population with a
327 prescribed variance in the aerosol module. The MOZ submodule describes the trace gas
328 chemistry from the troposphere to the lower thermosphere. The chemical mechanism includes

329 the O_x, NO_x, HO_x, ClO_x and BrO_x chemical families, along with CH₄ and its degradation
330 products. Several primary non-methane hydrocarbons (NMHCs) and related oxygenated
331 organic compounds are also described. It contains 108 species, 71 photolytic processes, 218
332 gas-phase reactions and 18 heterogeneous reactions with aerosol (Schultz et al., 2018). Details
333 of emissions (anthropogenic, biomass burning, biogenic, fossil fuel etc.) and model
334 parametrisation and other details are reported in the past Fadnavis et al. (2017, 2019a,b, 2021b).
335 Anthropogenic and biomass burning emissions of sulphate, and black carbon (BC) and organic
336 carbon (OC) are based on the AEROCOM-ACCMIP-II emission inventory for year 2020
337 (Lamarque et al., 2010; Textor et al., 2006). Additional consideration for the reduction of snow
338 albedo due to BC in snow is implemented but extended for the MOZ module. Snow albedo
339 reduction is calculated by considering the concentration of BC in the top layer of surface snow.
340 Influxes of BC in snow include below-cloud and in-cloud wet scavenging, as well as dry
341 deposition and sedimentation. Snowmelt and glacier runoff remove the in-snow BC at a
342 reduced efficiency, leading to enhanced concentration, while fresh and pristine snowfall leads
343 to reductions in BC concentration.

344

345 The model simulations were performed at T63 horizontal resolution ($1.875^\circ \times 1.875^\circ$) with 47
346 levels in the vertical from the surface to 0.01 hPa (corresponding to approx. 80 km), and with
347 a time step of 20 minutes. To understand the effect of the COVID-19 restrictions on snow over
348 Himalayas and Tibetan plateau region we conducted a control (CTL) and a COVID-19
349 (COVID) simulation. We adopted an ensemble approach (with 10 ensemble members) for the
350 above two experiments. Ten spin-up simulations were performed from 1 to 31 December 2019
351 to generate stabilised initial fields for the 10 ensemble members. Emissions were the same in
352 each of the 10 members during the spin-up period. Control simulations were extended with the
353 same setup until 1 June 2020. While for the COVID simulations (10 ensemble members each),

354 the anthropogenic emission of all gases and aerosols were changed since 1 January 2020
355 according to Google and Apple mobility data as in Forster et al. (2020). The COVID-19
356 emissions were prepared by deriving scaling factors between the input4MIPS SSP245 baseline
357 and the version5 of the Forster et al. (2020) 2-year blip scenario, separately for each species
358 and each grid point (see Fig. S5a). Subsequently, these scaling factors have been applied to the
359 AeroCom-II ACCMIP emissions. This ensures consistency of the drop in emissions
360 independent of the absolute emission values in the AeroCom-II ACCMIP and the input4MIPS
361 SSP245 data sets. The global mean emission changes in carbon monoxide (CO, 2-24%), black
362 carbon (BC, 3-23%), organic carbon (OC, 2-17%), sulfur dioxide (SO₂, 3-23%), nitrogen o
363 xides (NO_x, 2-30%), methane (CH₄, 2-5%), and ammonia (NH₃, 0-3%) during the period
364 January to 1 July 2020 (COVID - CTL) are in agreement with previous studies Forster et al.
365 (2020) and Le Quéré et al., (2020) (Fig. S5b). Our model experiments follow the CovidMIP
366 protocol (Jones et al., 2021). The COVID and CTL simulations ended on 1 June 2020. To
367 investigate the effects of COVID-19 emissions in spring (i.e., since 1 March 2020), we
368 analysed the difference between COVID and CTL simulations for the spring season in 2020.
369 The same dust parametrisation was employed in the CTL and COVID simulations.

370 A limitation of our simulation is the relatively coarse spatial resolution in the ECHAM6-
371 HAMMOZ model (1.875°x1.875°). Other studies used a finer spatially resolved regional
372 model; for example Sarangi et al. (2020) use a 12 x 12 km (~ 0.10°) grid in the regional WRF-
373 Chem-SNICAR model over the same region. In our model grid of 1.875°, many of the
374 Himalayan sub ranges are smaller than a pixel, and, hence, the topographic influences, which
375 are substantial in the mountains are limited. One effect may be that snowfall and snow on the
376 ground are underestimated (e.g., Liu et al., 2022). The coarse grid size can impact the anomalies
377 found here as the changes in snow mass are small, at most +16 mm, and the bias in the likely
378 underestimated snow mass may change between the control and COVID simulations. Biases

379 are, however, the same in the control and COVID simulations and, thus, their effects will be
380 diluted when we compute the anomalies.

381 **Section S2: Comparison of AOD over Western, Central, Eastern Himalayas and Tibetan**
382 **Plateau regions**

383 We elaborate on the comparison of MODIS AOD with our model simulations over
384 Western, Central, Eastern Himalayas and Tibetan Plateau regions (Fig. S6). Both MODIS and
385 the model show a reduction in AOD during spring 2020 over the aforementioned regions of
386 HKH. The estimated differences in AOD during March to May 2020 vary between 0.8 – 11%
387 over Western and Central Himalayas, and 8 – 16% over Eastern Himalayas. Over the Tibetan
388 plateau region, in contrast to the model simulations, MODIS shows an enhancement (2 – 16 %)
389 in AOD (Fig. S6). This may be due to dust aerosols, which are transported during spring from
390 western Asia and locally, generating dust piles over the Tibetan Plateau (Fadnavis et al., 2017,
391 2021a). The simulated dust aerosol concentration in spring 2020 over the Tibetan Plateau
392 region is smaller in the COVID than in the non-COVID (i.e. CTL) situation (Fig. S1c). The
393 changes in simulated dust are a response to meteorology difference between the COVID and
394 CTL simulations (Fig. S7).

395

396 References:

- 397 Bair, E., Stillinger, T., Rittger, K. & Skiles, M. COVID-19 lockdowns show reduced pollution
398 on snow and ice in the Indus River Basin. *Proc. Natl. Acad. Sci. U. S. A.* 118, 19–21,
399 <https://doi.org/10.1073/pnas.2101174118>, 2021. Bolch, T. *et al.* Status and Change of
400 the Cryosphere in the Extended Hindu Kush Himalaya Region. in *The Hindu Kush*
401 *Himalaya Assessment: Mountains, Climate Change, Sustainability and People* (eds.
402 Wester, P., Mishra, A., Mukherji, A. & Shrestha, A. B.) 209–255 (Springer International
403 Publishing). doi:10.1007/978-3-319-92288-1_7 2019, 2019.
- 404 Cruz, R.V., Harasawa, H., Lal, M., Wu, S, Anokhin, Y., Punsalmaa, B., Honda, Y., Jafari, M.,
405 Li, C., and Huu Ninh, N. Climate change 2001: impacts, adaptation, and vulnerability.
406 *Choice Rev. Online* 39, 39-3433-39–3433, 2007.
- 407 Fadnavis, S. Müller R., Chakraborty T., Sabin T. P., Laakso A., Rap A., Griessbach S., Vernier
408 J-P. & Tilmes S. The role of tropical volcanic eruptions in exacerbating Indian droughts.
409 *Sci. Rep.* 11, 1–13, <https://doi.org/10.1038/s41598-021-81566-0>, 2021.
- 410 Fadnavis, S., Müller R., Kalita G, Rowlinson M., Rap A., Frank Li J-L, Gasparini B, and
411 Laakso A., The impact of recent changes in Asian anthropogenic emissions of SO₂ on
412 sulfate loading in the upper troposphere and lower stratosphere and the associated
413 radiative changes, *ACP*, 19, 9989–10008, 2019a.
- 414 Fadnavis, S., Sabin T. P., Roy C., Rowlinson M, Rap A, Vernier J-P.& E. Sioris C. E.. Elevated
415 aerosol layer over South Asia worsens the Indian droughts. *Sci. Rep.* 9, 1–12,
416 <https://doi.org/10.1038/s41598-019-46704-9>, 2019b.
- 417 Fadnavis, S., Kalita, G., Ravi Kumar, K., Gasparini, B. & Li, J. L. F. Potential impact of
418 carbonaceous aerosol on the upper troposphere and lower stratosphere (UTLS) and
419 precipitation during Asian summer monsoon in a global model simulation. *Atmos.*
420 *Chem.Phys.* 17, 11637–11654, <https://doi.org/10.5194/acp-17-11637-2017>, 2017.

421 Fadnavis, S., Sabin T. P, Rap A., Müller R., Kubin A. and Heinold B., The impact of COVID-
422 19 lockdown measures on the Indian summer monsoon. *Environ. Res. Lett.* 16, DOI
423 10.1088/1748-9326/ac109c, 2021.

424 Forster, P. M. *et al.* Current and future global climate impacts resulting from COVID-19.
425 *Nat.Clim. Chang.* 10, 913–919, 2020.

426 Gogoi, M. M. S. Babu S., Arun B. S., Krishna, Moorthy K., Ajay A., Ajay P., Suryavanshi A.,
427 Borgohain A., *et al.* Response of Ambient BC Concentration Across the Indian Region
428 to the Nation-Wide Lockdown: Results from the ARFINET Measurements of ISRO-
429 GBP.*Curr. Sci.* 120, 341, doi: 10.18520/cs/v120/i2/341-351, 2021.

430 Hall, D. K. MODIS / Terra Snow Cover 5-Min L2 Swath 500m. *Color. USA NASA Natl. Snow*
431 *Ice Data Cent. Distrib. Act. Arch. Cent* 5, 2006.

432 Hock, R. *et al.* Chapter 2: High Mountain Areas. IPCC Special Report on the Ocean and
433 Cryosphere in a Changing Climate. *IPCC Spec. Rep. Ocean Cryosph. a Chang. Clim.*
434 131–202, 2019.

435 Huang, W. T. K. Aerosol effects on climate, with an emphasis on the Arctic.
436 <https://doi.org/10.3929/ethz-b-000319114> 2018, 2018.

437 Hussain, A. Sarangi G.K., Pandit A., Ishaq S., Mammun N., Ahmad B., Jamil M.K., Hydropower
438 development in the Hindu Kush Himalayan region: Issues, policies and opportunities.
439 *Renew. Sustain. Energy Rev.* 107, 446–461, <https://doi.org/10.1016/j.rser.2019.03.010>,
440 2019.

441 IPCC Working Group 1, I. *et al.* IPCC, 2013: Climate Change 2013: The Physical Science
442 Basis. Contribution of Working Group I to the Fifth Assessment Report of
443 the Intergovernmental Panel on Climate Change. *Ippc AR5*, 1535, 2013.

444 Jones, C. D., et al. The climate response to emissions reductions due to COVID-19: Initial
445 results from CovidMIP. *Geophysical Research Letters*, 48, e2020GL091883.
446 <https://doi.org/10.1029/2020GL091883>, 2021.

447 Kanniah, K. D., Kamarul Zaman, N. A. F., Kaskaoutis, D. G. & Latif, M. T. COVID-19's
448 impact on the atmospheric environment in the Southeast Asia region. *Sci. Total*
449 *Environ.* 736, 139658, <https://doi.org/10.1016/j.scitotenv.2020.1396580048-9697>, 2020.

450 Krishnan, R. *et al.* Assessment of climate change over the Indian region: A report of the
451 ministry of earth sciences (MOES), government of India. Assessment of Climate Change
452 over the Indian Region: A Report of the Ministry of Earth Sciences (MoES), Government
453 of India (Springer Singapore). doi:10.1007/978-981-15-4327-2, 2020.

454 Krishnan, R., Shrestha, A., Ren, G., Rajbhandari, R., Saeed, S., & Sanjay, J. Unravelling
455 Climate Change in the Hindu Kush Himalaya: Rapid Warming in the Mountains and
456 Increasing Extremes. *The Hindu Kush Himalaya Assessment* (Springer Singapore).
457 doi:10.1007/978-3-319-92288-1_3, 2019.1 , 2019.

458 Laakso A. The impact of recent changes in Asian anthropogenic emissions of SO₂ on sulfate
459 loading in the upper troposphere and lower stratosphere and the associated radiative
460 changes.. *Atmos. Chem. Phys.* 1–44, <https://doi.org/10.5194/acp-19-9989-2019>, 2019a.

461 Lamarque J.-F. , Bond T. C., Eyring V., Granier C., Heil A., Klimont Z., Lee D., Liousse C.,
462 Mieville A., Owen B., Schultz M. G., Shindell D., Smith S. J., Stehfest E., Aardenne J.
463 Van, Cooper O. R., Kainuma M., Mahowald N., McConnell J. R., Naik V., Riahi K., and
464 Vuuren D. P. van, Historical (1850-2000) gridded anthropogenic and biomass burning
465 emissions of reactive gases and aerosols: Methodology and application. *Atmos. Chem.*
466 *phys.* 10, 7017–7039, <https://doi.org/10.5194/acp-10-7017-2010>, 2010.

467 Lau, W. K. M., Kim, M. K., Kim, K. M. & Lee, W. S. Enhanced surface warming and
468 accelerated snow melt in the Himalayas and Tibetan Plateau induced by absorbing
469 aerosols. *Environ. Res. Lett.* 5, doi:10.1088/1748-9326/5/2/025204, 2010.

470 Le Quéré, C. Jackson R. B., M Jones M. W., Smith A. J. P., Abernethy S. Andrew R. M. , De-
471 Gol A. J. Willi D. R., Shan Y., Canadell J. G., Friedlingstein P., Creutzig F. and Peters
472 G. P., Temporary reduction in daily global CO2 emissions during the COVID-19 forced
473 confinement. *Nat. Clim. Chang.* 10, 647–653, [https://doi.org/10.1038/s41558-020-0797-](https://doi.org/10.1038/s41558-020-0797-x)
474 [x](https://doi.org/10.1038/s41558-020-0797-x)., 2020.

475 Lee, E., Carrivick1 J. L., Quincey D. J., Cook S. J., ames1 W. H. M., &. Brown L. E.,
476 Accelerated mass loss of Himalayan glaciers since the Little Ice Age. *Sci. Rep.* 11, 1–8,
477 <https://doi.org/10.1038/s41598-021-03805-8>, 2021b.

478 Lee, S. S., Chu, J. E., Timmermann, A., Chung, E. S. & Lee, J. Y. East Asian climate response
479 to COVID-19 lockdown measures in China. *Sci. Rep.* 11, 1–9, 2021a.

480 Liu, Y. Wang Y. , Cao Y., Yang Xi, T Zhang T., Luan M., Lyu D., Hansen A. D. A., Liu B., and
481 Liu, Y., Fang, Y., Li, D., and Margulis, S. A.: How Well do Global Snow Products Characterize
482 Snow Storage in High Mountain Asia?, *Geophysical Research Letters*, 49,
483 e2022GL100082, <https://doi.org/10.1029/2022GL100082>, 2022.

484 Ma, J. Zhang T., and GUAN X., The dominant role of snow/ice Albedo feedback strengthened
485 by black carbon in the enhanced warming over the Himalayas. *J. Clim.* 32, 5883–5899,
486 <https://doi.org/10.1175/JCLI-D-18-0720.s1.2019>.

487 Martonchik, J. V., Diner, D. J., Kahn, R., Gaitley, B. & Holben, B. N. Comparison of MISR
488 and AERONET aerosol optical depths over desert sites. *Geophys. Res. Lett.* 31, 1–4,
489 <https://doi.org/10.1029/2004GL019807>, 2004.

490 Nair, V. S. Babu S. S., Moorthy K. K., Sharma A. K., Marinoni A. & Ajai, Black carbon aerosols
491 over the Himalayas: Direct and surface albedo forcing. *Tellus, Ser. B Chem. Phys.*
492 *Meteorol.* 468 65, DOI: 10.3402/tellusb.v65i0.19738, 2013.

493 Pandey, S. K. & Vinoj, V. Surprising changes in aerosol loading over india amid covid-19
494 lockdown. *Aerosol Air Qual. Res.* 21, 1–12, <https://doi.org/10.4209/aaqr.2020.07.0466>,
495 2021.

496 Qian, Y., Flanner, M. G., Leung, L. R. & Wang, W. Sensitivity studies on the impacts of
497 Tibetan Plateau snowpack pollution on the Asian hydrological cycle and monsoon
498 climate. *Atmos. Chem. Phys.* 11, 1929–1948, doi:10.5194/acp-11-1929-2011, 2011.

499 Rogelj, J. Schaefferc M., Meinshausene M., Shindell D. T, Harec W., Klimontb Z., Veldersh
500 G. J. M., Amannb M., and Schellnhuberr H.J., Disentangling the effects of CO2 and short
501 lived climate forcer mitigation. *Proc. Natl. Acad. Sci. U. S. A.* 111, 16325–16330,
502 <https://doi.org/10.1073/pnas.1415631111>, 2014.

503 Sabin, T., Krishnan, R., Vellore, R., Priya, P., Borgaonkar, H., Singh, B., Sagar, A. Droughts
504 and floods. *Climate Change Over the Himalayas. Assessment Of Climate Change Over*
505 *The Indian Region.* doi:10.1007/978-981-15-4327-2_11, 2020.

506 Santra, S. Verma1 S., Fujita K, Chakraborty I, Boucher O., Takemura T., Burkhardt John F.,
507 Matt F, and Sharma M., Simulations of black carbon (BC) aerosol impact over Hindu
508 Kush Himalayan sites: Validation, sources, and implications on glacier runoff. *Atmos.*
509 *Chem. Phys.* 19, 2441–2460, <https://doi.org/10.5194/acp-19-2441-2019>, 2019.

510 Sarangi, C. Qian Y., Rittger K., Bormann K.J., Liu Y., Wang H., Wan H., Lin G., and. Painter
511 T.H., Impact of light-absorbing particles on snow albedo darkening and associated
512 radiative forcing over high-mountain Asia: high-resolution WRF-Chem modeling and
513 new satellite observations. *Atmos. Chem. Phys.* 19, 7105–7128,
514 <https://doi.org/10.5194/acp-19-7105-2019>, 2019.

515 Sarangi, C., Qian, Y., Rittger, K., Ruby Leung, L., Chand, D., Bormann, K. J., and Painter, T.
516 H.: Dust dominates high-altitude snow darkening and melt over high-mountain Asia,
517 Nature Climate Change, 10, 1045-1051, 10.1038/s41558-020-00909-3, 2020.

518 Schultz, M. G., Stadtler S., Schröder S., Taraborrelli D., Franco B., Krefting J, Henrot A. et al.,
519 The chemistry-climate model ECHAM6.3-HAM2.3-MOZ1.0. *Geosci. Model Dev.* 11,
520 1695–1723, <https://doi.org/10.5194/gmd-11-1695-2018>, 2018.

521 Shafeeque, M. Arshad A., A Elbeltagi A., Sarwar A., Pham Q. B., S Khan S. N., I Dilawar A.
522 & Al-Ansari N., Understanding temporary reduction in atmospheric pollution and its
523 impacts on coastal aquatic system during COVID-19 lockdown: a case study of South
524 Asia. *Geomatics, Nat. Hazards Risk* 12, 560–580,
525 <https://doi.org/10.1080/19475705.2021.1885503>, 2021.

526 Srivastava, A. K., Bhojar P.D., K 499 anawade V. P., Devara P.C. S., Thomas A., Soni V.K.,
527 Improved air quality during COVID-19 at an urban megacity over the Indo-Gangetic
528 Basin: From stringent to relaxed lockdown phases. *Urban Clim.* 36, 100791,
529 <https://doi.org/10.1016/j.uclim.2021.100791>, 2021.

530 Stevens, B., Giorgetta M., Esch M., Mauritsen T., Crueger T., Rast S., Salzmann M., Schmidt
531 H., Bader J., Block K., Brokopf R., Fast I., Kinne S., Kornblueh L., Lohmann U., Pincus
532 R., Reichler T., Roeckner E. Atmospheric component of the MPI-M earth system model:
533 ECHAM6. *J. Adv. Model. Earth Syst.* 5, 146–172, <https://doi.org/10.1002/jame.20015>,
534 2013.

535 Stier, P., Feichter J., Kinne S., Kloster S., Vignati E., Wilson J., Ganzeveld L., Tegen I., Werner
536 M., Balkanski Y. Schulz M., Boucher O., Minikin A., and Petzold A., The aerosol-climate
537 model ECHAM5-HAM. *Atmos. Chem. Phys.* 5, 1125–1156, [https://doi.org/10.5194/acp-](https://doi.org/10.5194/acp-5-1125-2005)
538 [5-1125-2005](https://doi.org/10.5194/acp-5-1125-2005), 2005.

539 Tegen, I., Neubauer D., Ferrachat S., Siegenthaler-Le Drian C, Bey, I., Schutgens N., Stier P.,
540 Watson-Parris D., et al., The global aerosol-climate model echam6.3-ham2.3 -Part 1:
541 Aerosol evaluation. *Geosci. Model Dev.* 12, 1643–1677, [https://doi.org/10.5194/gmd-12-](https://doi.org/10.5194/gmd-12-1643-2019)
542 1643-2019, 2019.

543 Textor , Schulz M, Guibert S., Kinne S., Balkanski Y., Bauer S., Berntsen T., Berglen T.,
544 Boucher O., Chin M., Dentener F, Diehl T., Easter R., Feichter H., Fillmore D., Ghan
545 S., Ginoux P., Gong S., Grini A., Hendricks J. , Horowitz L., Huang P., Isaksen I., Iversen
546 I, Kloster S., Koch D., Kirkevåg A., Kristjansson J. E., Krol M., Lauer A., Lamarque J.
547 F., Liu X., Montanaro V., Myhre G., Penner J., Pitari G., Reddy S., Seland Ø., Stier P.,
548 Takemura T., and Tie X., Analysis and quantification of the diversities of aerosol life
549 cycles within AeroCom. *Atmos. Chem. Phys.* 6, 1777–1813, [https://doi.org/10.5194/acp-](https://doi.org/10.5194/acp-6-1777-2006)
550 6-1777-2006, 2006.

551 Thind, P. S., Chandel, K. K., Sharma, S. K., Mandal, T. K. & John, S. Light-absorbing
552 impurities in snow of the Indian Western Himalayas: impact on snow albedo, radiative
553 forcing, and enhanced melting. *Environ. Sci. Pollut. Res.* 26, 7566–7578,
554 <https://doi.org/10.1007/s11356-019-04183-5>, 2019.

555 Tiwari, S., Kar, S. C. & Bhatla, R. Snowfall and Snowmelt Variability over Himalayan Region
556 in Inter-annual Timescale. *Aquat. Procedia* 4, 942–949,doi:
557 10.1016/j.aqpro.2015.02.118, 2015.

558 Usha, K. H., Nair, V. S. & Babu, S. S. Effect of aerosol-induced snow darkening on the direct
559 radiative effect of aerosols over the Himalayan region. *Environ. Res. Lett.* 16,
560 <https://doi.org/10.1088/1748-9326/abf190>, 2021.

561 Wester P., Mishra A., Mukherji A., S. A. B. The Hindu Kush Himalaya Assessment—
562 Mountains, Climate Change, Sustainability and People. Springer Nature Switzerland AG,
563 Cham. doi:<https://doi.org/10.1007/978-3-319-92288-1>, 2019.

564 Wood, L. R. Neumann K., Nicholson K.N., Bird B.W., Dowling C. B. and Sharma S.. Melting
565 Himalayan Glaciers Threaten Domestic Water Resources in the Mount Everest Region,
566 Nepal. *Front. Earth Sci.* 8, 1–8, <https://doi.org/10.3389/feart.2020.00128>, 2020.

567 Zhang, K. O'Donnell D., Kazil J., Stier P., Kinne S., Lohmann U., Ferrachat S., Croft B., Quaas
568 J, Wan H., Rast S., and Feichter J., The global aerosol-climate model ECHAMHAM,
569 version 2: Sensitivity to improvements in process representations. *Atmos. Chem.Phys.*
570 12, 8911–8949, <https://doi.org/10.5194/acp-12-8911-2012>, 2012.

571 Zheng M., Impacts of COVID-19 on Black Carbon in Two Representative Regions in China:
572 Insights Based on Online Measurement in Beijing and Tibet. *Geophys. Res. Lett.* 48, 1–
573 11, [10.1029/2021GL092770](https://doi.org/10.1029/2021GL092770), 2021.

574

575 **Acknowledgments**

576 The authors thank the staff of the High Power Computing Centre (HPC) in IITM, Pune, India,
577 for providing computer resources and the team members of MODIS for providing data. We
578 thank Sabur F. Abdullaev and Brent Holben for their efforts in establishing and maintaining
579 Dushanbe and Lahore AERONET sites respectively. Work done in the manuscript is not
580 supported by any funding agency.

581 **Funding information**

582 The manuscript is not funded.

583 **Author Contributions**

584 S.F. initiated the idea of the study. S.F. and B. H. performed model simulations. A.R. and A.
585 K. prepared Google based emission inventory. T.P.S., A.A., R.M. performed data analysis and
586 contributed in overall design. All authors contributed to discussions of the results and the
587 writing of the manuscript.

588 **Data and code availability**

589 The ECHAM-HAMMOZ model source code and all required input data are available to the
590 scientific community according to the HAMMOZ Software License Agreement through the
591 project website: <https://redmine.hammoz.ethz.ch/projects/hammoz>. The data that support the
592 findings of this study are openly available in zenodo at <http://doi.org/.../zenodo...>

593

594 **Competing Interests:** The authors declare no competing interests.